

# Kinetic and Docking Studies of the Interaction of Quinones with the Quinone Reductase Active Site<sup>†</sup>

Zhigang Zhou,<sup>‡</sup> Derek Fisher,<sup>§</sup> Jared Spidel,<sup>§</sup> Jodi Greenfield,<sup>§</sup> Brian Patson,<sup>§</sup> Aleem Fazal,<sup>§</sup> Carl Wigal,<sup>§</sup> Owen A. Moe,<sup>\*,§</sup> and Jeffry D. Madura<sup>\*,‡</sup>

*Department of Chemistry, Lebanon Valley College, Annville, Pennsylvania 17003, and  
Department of Chemistry and Biochemistry, Duquesne University, Pittsburgh, Pennsylvania 15282*

*Received July 25, 2002; Revised Manuscript Received November 5, 2002*

**ABSTRACT:** NAD(P)H/quinone acceptor oxidoreductase type 1 (QR1) protects cells from cytotoxic and neoplastic effects of quinones through two-electron reduction. Kinetic experiments, docking, and binding affinity calculations were performed on a series of structurally varied quinone substrates. A good correlation between calculated and measured binding affinities from kinetic determinations was obtained. The experimental and theoretical studies independently support a model in which quinones (with one to three fused aromatic rings) bind in the QR1 active site utilizing a  $\pi$ -stacking interaction with the isoalloxazine ring of the FAD cofactor.

NAD(P)H:quinone acceptor oxidoreductase type 1 (QR1,<sup>1</sup> EC 1.6.99.2), a homodimeric flavoprotein of 273 residues ( $M = 30815$ ) per monomer, catalyzes an obligatory two-electron reduction of quinones using either NADH or NADPH as electron donors (*1, 2*). QR1 affords protection against the cytotoxic and neoplastic effects of electrophilic quinones and partially reduced semiquinones that can undergo redox cycling to generate active oxygen species (*3*). QR1, found in many solid tumors at elevated levels, can be used to target the tumor cells through bioreductive activation of quinone-based chemotherapeutic agents (*3*).

The crystal structures of quinone reductases from rat (PDB ID: 1QRD), mouse (1DXQ), and human (1DXO, 1D4A), reflecting a high degree of sequence identity, show very small differences in the positions of the 220  $\alpha$ -carbons in the catalytic domain and possess nearly identical active sites (*1, 4, 5*). The crystal structure for the rat enzyme (1QRD) contains duroquinone, FAD, and the NAD(P)H analogue cibracon blue, but the latter ligand sterically intrudes into the active site, affecting the position of at least one key residue, Tyr128 (*1, 4*). The human enzyme, whose crystal structure (1DXO) contains duroquinone and FAD but no cibracon blue, differs from the rat enzyme by one amino acid (Gln104 in human, Tyr104 in rat) in the active site, resulting in a slight change (0.7 Å) in the positioning of the flavin ring (*1*).

The quinone reductase active site, produced by residues from each subunit of the dimeric protein, has the following features: (1) the duroquinone overlays the FAD isoalloxazine ring that is bound to one subunit, with the quinoid carbonyl oxygens oriented roughly parallel to the length of the flavin ring; (2) a loop from the second subunit, which forms a lid for the active site above the bound quinone, provides two tyrosine residues, Tyr126 and Tyr128, that hydrogen bond directly, or indirectly via a water molecule, to the quinone carbonyl groups; and (3) three aromatic residues provide hydrophobic contacts with the quinone, and one of these, Trp105, forms a wall bordering one side of the active site (*1*). A depiction of the human quinone reductase (1DXO) active site is shown in Figure 1.

Mechanistically, a hydride ion from NAD(P)H is thought to be transferred to the flavin nitrogen, N<sup>5</sup>, with possible charge stabilization from a catalytic triad involving the FAD, Tyr155, and His161 (*4*). The hydride would then be donated from N<sup>5</sup> to the quinone substrate at either a carbonyl oxygen or a ring carbon, with the remaining proton coming from Tyr126 or H<sub>2</sub>O/Tyr128, acting as general acids.

The work presented here correlates kinetic data collected for a series of structurally varied quinone substrates with predictions of active site positioning and binding energies from theoretical docking studies. The kinetic and docking studies independently support a model in which quinones with one to three fused aromatic rings in the quinone nucleus interact with the active site so as to optimize  $\pi$ -ring-stacking interactions with the isoalloxazine ring of the FAD cofactor, even though such optimization means changing the orientation and reactivity of the quinoid carbonyl oxygens. Hydrogen-bonding interactions with Tyr126 and Tyr128 are also important determinants of binding strength.

## EXPERIMENTAL PROCEDURES

**Materials.** NADH, Tween-20, MTT [3-(4,5-dimethylthiazol-2-yl)-2,5-diphenyl-2H-tetrazolium bromide], 1,4-benzo-

<sup>†</sup> This work was supported by Grants NSF 9974789 (to Duquesne University) and SF-98-005 from the Camille and Henry Dreyfus Foundation (to Lebanon Valley College).

<sup>\*</sup> To whom correspondence should be addressed. O.A.M.: phone, (717) 867-6144; fax, (717) 867-6124; e-mail, moe@lvc.edu. J.D.M.: phone, (412) 396-6341; fax, (412) 396-5683; e-mail, madura@duq.edu.

<sup>‡</sup> Duquesne University.

<sup>§</sup> Lebanon Valley College.

<sup>1</sup> Abbreviations: QR1, NAD(P)H/quinone acceptor oxidoreductase type 1; BFE, binding free energy; MOE, molecular operating environment; SD, standard deviation.

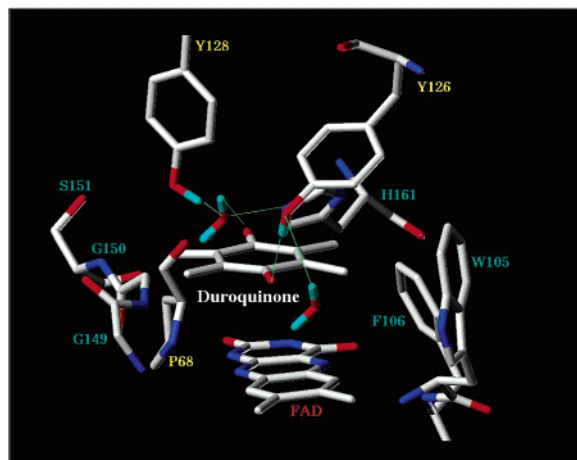


FIGURE 1: Depiction of the QR1 active site (1DXO) created on Bipolymer from Tripos. The duroquinone ring stacks 3.5 Å above the flavin ring, with carbonyl oxygens running almost parallel with the length of the isoalloxazine ring. One quinoid carbonyl forms a hydrogen bond with a water molecule, which in turn hydrogen bonds to Y128 and H161. The other carbonyl hydrogen bonds to Y126. Residues from different subunits are identified by blue and yellow lettering.

quinone, 1,4-naphthoquinone, 1,2-naphthoquinone, 2-methyl-1,4-naphthoquinone, 9,10-anthraquinone, and 1,4-anthraquinone were purchased from Aldrich/Sigma. 2,3-Dimethyl-1,4-naphthoquinone, 2-ethyl-1,4-naphthoquinone, 2-*n*-propyl-1,4-naphthoquinone, 2-isopropyl-1,4-naphthoquinone, and 2-*n*-butyl-1,4-naphthoquinone were synthesized using modifications of a published procedure (6). Other chemicals are commonly available. Quinone reductase was purified from rat liver using cibracon blue–agarose affinity chromatography using an established method (7).

**Kinetic Determinations.** Two types of assays were used to measure the reaction kinetics. The first assay, which followed the oxidation of NADH at 340 nm (8), was used with substrates giving quinone Michaelis constant ( $K_Q$ ) values  $>50 \mu\text{M}$ . The second assay, used for substrates of  $K_Q < 50 \mu\text{M}$ , measured the reduction of MTT at 610 nm as MTT reoxidized hydroquinone to regenerate the oxidized quinone (9). Conditions for kinetic assays were 25 °C, 0.025 M Tris-HCl, pH 7.40, 725  $\mu\text{M}$  MTT (when used), 200  $\mu\text{M}$  NADH, 0.067% BSA, 0.001% Tween-20, and 2.4% v/v ethanol. Quinones were dissolved in 95% ethanol for addition to the reaction cuvette. The low aqueous solubility of the quinones studied and the inactivation of the enzyme at ethanol concentrations above 2.4% limited the maximal concentrations of quinone substrates to a range of 100–200  $\mu\text{M}$ .

**Solvation Energies.** Calculations of aqueous solvation energies were performed using Gaussian 98 (Gaussian, Inc) packages for ab initio calculations. The geometry optimizations and energy calculations were carried out using the HF/6-31G\* level of theory, and solvation effects were treated by IPCM (10, 11) models. The IPCM model used a dielectric constant of 78. The HF energy difference between the gas phase and aqueous state is used for solvation energy.

**Docking.** The molecular operating environment (MOE) program (Chemical Computing Group) was used to perform molecular building, coordinate preparation, docking, and calculations of solvation energies and relative binding free energies. Autodock3 (12) also was used for docking and relative binding free energy calculations. MOE dock utilizes

a Monte Carlo simulated annealing (SA) method in docking calculations to search for favorable binding configurations of a small, flexible ligand and a rigid macromolecule in a preset box. By generating random changes to the ligand's coordinates, the dock searches in the box and calculates docking energies on the basis of a grid in the box. In Autodock3, SA and genetic algorithm (GA) methods are available. As the Lamarckian genetic algorithm (LGA) showed better performance than SA on reproducing a crystal complex (13), the LGA was used in Autodock3 to perform docking and relative binding free energy calculations. The hybrid search technique consists of a global optimizer modified from the genetic algorithm with two-point crossover and random mutation and a local optimizer with a Solis and Wets algorithm (14). Autodock3 calculates the binding free energy on the basis of the assumption that the binding free energy change equals the binding free energy in a vacuum plus the solvation free energy difference between complexed and free individual molecules.

In MOE dock, a docking box of  $60 \times 40 \times 40$  points with a grid spacing of 0.375 Å was placed around the active site of the protein. The substrate begins outside the entrance of the active site. The iteration limit was set to 20000, the number of cycles was set to 20, and the number of runs was set to 20. So a total of 20 docking configurations were determined in each docking calculation.

In Autodock3, a docking box of  $60 \times 60 \times 60$  points with a grid spacing of 0.375 Å was used in the calculations. In the LGA setting, random was used in seed, initial quaternion, coordinates, and torsions. The translation step was set to 0.2 Å. Quaternion and torsion steps were set to 25°. The GA\_r number of individuals in the population was set to 50. The maximum number of energy evaluations was 250000. The maximum number of generations was 27000. The rate of gene mutation was 0.02, and the rate of crossover was 0.8.

**Binding Free Energy Based on Poisson–Boltzmann Solvation Energy.** As suggested by Gilson and Honig (15), the binding free energy can be partitioned into solvation energies,  $\Delta G_s$ , assembly energies,  $\Delta G_a$ , and nonelectrostatic energies,  $\Delta G_n$ :

$$\Delta G = \Delta G_s(\text{bound}) - \Delta G_s(\text{free}) + \Delta G_a(\text{bound}) - \Delta G_a(\text{free}) + \Delta G_n(\text{bound}) - \Delta G_n(\text{free})$$

$$\Delta G_s(\text{bound}) = \Delta G_s(\text{LP}) - \Delta G_s(\text{L}) - \Delta G_s(\text{P})$$

$$\Delta G_a(\text{bound}) = \Delta G_a(\text{LP}) - \Delta G_a(\text{L}) - \Delta G_a(\text{P})$$

$$\Delta G_n(\text{bound}) = \Delta G_n(\text{LP}) - \Delta G_n(\text{L}) - \Delta G_n(\text{P}) \quad (1)$$

where LP is used to represent the protein–ligand complex, L represents the ligand, and P represents the protein.

Solvation energies were calculated by the Poisson–Boltzmann equation (16–20) as implemented in MOE statistics. For the vacuum calculations we used an interior dielectric constant of 3 and an outer dielectric constant of 1, while for the solvent calculation a value of 3 was used for the interior dielectric and 78 for the exterior dielectric constants. A solution of 0.1 NaCl was used as the solvent. Other default settings were used. A grid spacing of 0.75 was used in the calculations.

The assembly energy,  $\Delta G_a$ , was calculated using a standard molecular mechanics force field and a dielectric constant was used. The nonelectrostatic energy was estimated by the solvent-accessible surface model (21).

**Coordinate Preparation.** The coordinates for quinone reductase (1DXO) were downloaded from the Protein Data Bank. The physiological dimer in the crystal unit was used in all calculations. We performed docking calculations using one of the two identical active sites. Two crystallographic water molecules were removed from the active site before docking since they could block a substrate from docking. Hydrogen atoms and partial charges were added to the enzyme by MOE using the Kollman94 force field. MOE used the PEOE method to assign partial charges for the FAD cofactors and duroquinone (22–24). After all non-hydrogen atoms were fixed, the molecule was energy minimized by a combination minimization method comprised of steepest descent, conjugate gradient, and truncated Newton (25). The minimized coordinates of 1DXO were used in the docking and relative free energy of binding calculations. After PEOE partial charges were assigned to the quinone substrates, energy minimizations were performed to relax the substrates prior to docking.

In MOE docking, the initial position of a substrate for docking was outside the entrance of the active site. Since Autodock3 uses the substrate as reference to decide the grid coordinates, the coordinates of duroquinone were used as the initial position for the docking calculation. The other substrates were superimposed on the duroquinone to obtain their initial positions.

## RESULTS AND DISCUSSION

### Kinetic Study of Quinone Substrates

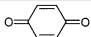
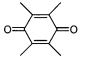
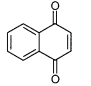
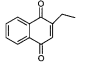
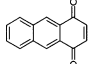
**Effect of the Number of Fused Rings in the Quinone Nucleus.** The quinone reductase bisubstrate reaction proceeds via a ping-pong double-displacement mechanism in which the oxidized quinone substrate competitively inhibits NADH binding (26). The rate law for this mechanism, shown in eq 2, includes  $K_Q$  and  $K_N$ , Michaelis constants for the quinone and NADH substrates, as well as  $K_{iQ}$ , an inhibition constant for the quinone substrate.

$$v = \frac{V}{1 + \frac{K_Q}{[Q]} + \frac{K_N}{[NADH]} \left(1 + \frac{[Q]}{K_{iQ}}\right)} \quad (2)$$

In our kinetic analyses, a literature value of 36.2  $\mu\text{M}$  was used for  $K_N$  (27), and best fit values for the remaining kinetic constants were determined by nonlinear regression analysis of substrate saturation data. We observed substrate inhibition with all quinone substrates, but inhibition was generally weak within the limited solubility range of the quinone substrates. Best fit values for  $K_{iQ}$  therefore carried a higher degree of uncertainty than the more precisely determined values for  $K_Q$  and  $V$ .

Kinetic data for quinone substrates having one, two, and three fused rings in the quinone nucleus are compared in Table 1. As the number of fused rings increases from one to three, the quinone Michaelis constants decrease 100-fold and the maximal velocities decrease by 88%. Small alkyl

Table 1: Kinetic Effect of the Number of Fused Rings in the Quinone Nucleus

Substrate	# of rings	$K_Q (\pm \text{SD}) \mu\text{M}$	$V (\pm \text{SD})$ relative <sup>a</sup>	$\Delta G_{\text{solv}}$ <sup>b</sup>
			%	kcal/mol
 Benzoquinone	1	90( $\pm$ 12)	264( $\pm$ 19)	-10.1
 Duroquinone	1	84( $\pm$ 13)	260( $\pm$ 11)	-7.7
 1,4-naphthoquinone	2	3.3( $\pm$ 1.6)	100( $\pm$ 3)	-12.7
 2-ethyl-1,4-naphthoquinone	2	2.7( $\pm$ 0.9)	89( $\pm$ 11)	-10.8
 1,4-anthraquinone	3	0.91( $\pm$ 0.31)	31( $\pm$ 5)	-15.0

<sup>a</sup> All maximal velocities normalized to that of 1,4-naphthoquinone; SD, standard deviation. <sup>b</sup> Calculated using the IPCM model.

substituents on the quinone nucleus appear to have little effect, if any, on either the  $K_Q$  or the  $V$  values.

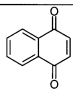
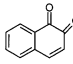
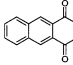
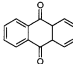
In the case that the rate constant for the transfer of the hydride from the reduced flavin to the quinone is rate limiting,  $K_Q$  becomes equal to the dissociation constant for the reduced enzyme–quinone complex. Since [NADH] is constant in all determinations in Table 1, the observed 88% decrease in maximal velocity argues that it is quinone reduction, rather than NADH oxidation in the first portion of the ping-pong mechanism, that is rate limiting in the series of substrates that we have selected. We will therefore assume the  $K_Q$  parameters determined here to be quantitative indicators of substrate binding affinity to the enzyme active site.

It is possible that the observed 100-fold decrease in  $K_Q$  is due to a general hydrophobic effect in which an increase in the number of fused aromatic rings produces less favorable free energies of interactions with the polar aqueous solvent, thereby driving the larger quinones from the bulk aqueous solvent into a hydrophobic active site on the enzyme surface. The calculated free energies of solvation,  $\Delta G_{\text{solv}}$ , in Table 1 are, however, not consistent with such an explanation.

One possible mechanism by which the larger quinones could gain binding energy would be through  $\pi$ -ring stacking with the isoalloxazine ring of the flavin (28). From the positioning of the duroquinone substrate in the crystal structure, it is clear that ring stacking of the naphtho- and anthraquinones would require a ca. 90° rotation of the carbonyl bond axis of the quinone substrates. Such a repositioning would move the carbonyls relative to the hydride donor on the flavin ring and relative to the Tyr126 and Tyr128 general acid catalysts, potentially affecting the catalytic rate. A change in positioning to achieve ring



Table 2: Kinetic Effect of Carbonyl Positioning in the Quinone Nucleus

Substrate	$K_Q (\pm SD) \mu M$	$V (\pm SD)$ relative %	$K_i (\pm SD) \mu M$
	3.3( $\pm 1.6$ )	100( $\pm 3$ )	ND
1,4-naphthoquinone			
	82( $\pm 29$ )	178( $\pm 7$ )	ND
1,2-naphthoquinone			
	0.91( $\pm 0.31$ )	31( $\pm 5$ )	ND
1,4-antraquinone			
	ND	$< 0.10$	80( $\pm 25$ )
9,10-antraquinone			

stacking could, then, explain the changes both in Michaelis constants and in maximal velocities seen in Table 1.

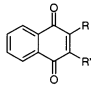

**Effect of Quinone Carbonyl Position.** Kinetic comparisons between two substrate pairs, 1,4- and 1,2-naphthoquinone and 1,4- and 9,10-antraquinones, are given in Table 2. In the naphthoquinone system, shifting from the *p*- to *o*-carbonyls causes a 25-fold increase in  $K_Q$  and an almost 2-fold increase in maximal velocity. For the anthraquinone system, moving the quinone carbonyls to the middle ring results in a complete loss of catalytic activity, making  $K_Q$  determination impossible. We were, however, able to carry out a study of 9,10-antraquinone as a competitive inhibitor of 1,4-naphthoquinone. Inhibition, though weak, gave an inhibition constant,  $K_i$ , of 80 ( $\pm 25$ )  $\mu M$  for 9,10-antraquinone. This  $K_i$  is close in value to a Michaelis constant ( $K_Q = 43 \mu M$ ) measured for the structurally similar 1,4-dihydroxy-9,10-antraquinone (29).

**Effect of Alkyl Substituents.** A determination of the effect of alkyl substitution on the quinone reductase kinetic parameters is given in Table 3. In this study, 1,4-naphthoquinone was substituted with alkyl groups ranging from one to six carbons. In contrast to the results from the fused ring study, the addition of alkyl substituents to the two-ring quinoid nucleus produces only small effects on the measured kinetic parameters, with  $K_Q$  and  $V$  values usually differing by less than a factor of 2 over the entire set of compounds.

The kinetic studies indicate that addition of fused aromatic rings to the quinone nucleus can measurably affect both substrate binding and the rate of catalysis. The data suggest that the quinone carbonyl positioning may change as more fused rings are added. Changing the carbonyl positioning within a particular nucleus also has a measurable kinetic effect, especially within the anthraquinone system. Adding more flexible alkyl groups, however, seems to produce much smaller kinetic effects.

To understand the effects of quinone structural changes on quinone reductase reaction kinetics, we undertook a docking study to determine the predicted positioning and relative interaction energies of quinone ligands at the active

Table 3: Kinetic Effect of Alkyl Substitution on 1,4-Naphthoquinone

	$K_Q (\pm SD) \mu M$	$V (\pm SD)$ relative %
Substituted naphthoquinone substrate		
R=H, R'=H	3.3( $\pm 1.6$ )	100( $\pm 3$ )
R= -CH <sub>3</sub> , R'=H	3.1( $\pm 2.3$ )	115( $\pm 4$ )
R= -CH <sub>2</sub> CH <sub>3</sub> , R'=H	2.7( $\pm 0.9$ )	89( $\pm 11$ )
R= -CH <sub>3</sub> , R'= -CH <sub>3</sub>	3.9( $\pm 1.6$ )	149( $\pm 7$ )
R= -CH <sub>2</sub> CH <sub>2</sub> CH <sub>3</sub> , R'=H	3.6( $\pm 0.5$ )	64( $\pm 1$ )
R= -CH(CH <sub>3</sub> )CH <sub>3</sub> , R'=H	7.0( $\pm 1.6$ )	79( $\pm 17$ )
R= -CH <sub>2</sub> (CH <sub>2</sub> ) <sub>2</sub> CH <sub>3</sub> , R'=H	6.8( $\pm 1.2$ )	65( $\pm 4$ )
R=  , R'=H	6.0( $\pm 1.2$ )	69( $\pm 6$ )

site of quinone reductase. A crystal structure is available for the rat liver quinone reductase (1QRD), a structure that contains FAD, duroquinone, and cibracon blue (4). Comparisons of the rat quinone reductase structure with crystal structures of mouse and human quinone reductases indicate that the cibracon blue dye bound in the rat enzyme causes a distortion of the active site (1).

We therefore chose for our modeling studies 1DXO, the crystal coordinates for a human quinone reductase complex containing FAD and duroquinone. The rat and human enzymes have virtually identical active sites, differing mainly by a mutation in which Tyr104 in rat is replaced by Gln104 in the human enzyme (30). We have concluded that, for our analyses, the human enzyme provides a better model of the quinone reductase active site than does the distorted rat crystal structure.

### Docking Studies

**Validation.** To validate the MOE-dock method, we docked duroquinone back into the active site. The MOE-dock method we used employed 20 different determinations, each using a random initial placement of the duroquinone within the active site. For duroquinone, all 20 final docked positions of the substrate fell within a single cluster, where a cluster is defined as a group of positions that gives a RMS deviation of  $< 1 \text{ \AA}$  for the quinone carbon and oxygen atoms. Shown in Table 4 are duroquinone docking results in which data are reported only for the five docked orientations of lowest energy. The docking energy for the one lowest energy orientation of duroquinone is  $-33.18 \text{ kcal/mol}$ . For the other orientations, the difference in energy between each specific orientation and the lowest energy orientation is given. For duroquinone, for example, the first and fifth lowest energy docked orientations differ by only  $1.16 \text{ kcal/mol}$ . The RMS deviations in the carbon and oxygen atomic positions between the lowest energy and four other orientations are also given in Table 4. For duroquinone, the largest RMS deviation among the five lowest energy orientations is  $0.089 \text{ \AA}$ . The lowest energy orientation of docked duroquinone is shown in Figure 2A relative to the isoalloxazine ring of the

Table 4: Energy and Position Difference between Several Best Docked Configurations of Each Substrate by MOE Dock

	cluster	no. in cluster <sup>a</sup>	$\Delta E^b$ (kcal/mol)	RMSD <sup>c</sup> (Å)
duroquinone	1	20	0.13	0.015
			0.30	0.066
			0.82	0.089
benzoquinone	1	11	1.16	0.073
			0.02	0.026
			0.08	0.027
			0.15	0.030
	2	9	0.18	0.029
			0.03	0.032
1,4-naphthoquinone	1	16	0.03	0.520
			0.04	0.436
			0.04	0.321
			0	0.055
	2	4	0.13	0.077
			0.13	0.019
1,2-naphthoquinone	1	19	0.14	0.041
			0.16	0.042
			0.18	0.054
			0.26	0.062
	2	1	0	0.033
			0.04	0.024
2-cyclohexyl-1,4-naphthoquinone	1	10	0.08	0.041
			0.09	0.041
			0.21	0.155
			0.23	0.128
	2	10	0.27	0.045
			0.79	0.103
2-propyl-1,4-naphthoquinone	1	13	1.75	0.272
			1.76	0.092
			1.78	0.103
			1.86	0.114
	2	7	0.03	0.188
			0.29	0.625
1,4-anthraquinone	1	20	0.42	0.590
			0.47	0.610
			0.09	0.596
			0.14	0.612
	2	14	0.18	0.620
			0.20	0.576
9,10-anthraquinone	1	20	0.13	0.020
			0.17	0.026
			0.18	0.038
			0.20	0.042
	2	6	0.01	0.008
			0.01	0.006
2,3-dimethyl-1,4-naphthoquinone	1	14	0.07	0.014
			0.11	0.011
			0.20	0.042
			0.0	0.021
	2	6	0.01	0.034
			0.01	0.12
			0.13	0.11
			0.03	0.09
			0.04	0.13
			0.03	0.08

<sup>a</sup> The number of configurations falling in the cluster. <sup>b</sup>  $\Delta E = E_i - E_{\text{lowest}}$ . <sup>c</sup> RMSD, root-mean-square deviation between the docked structure and the lowest docked structure. <sup>d</sup> Substrate is parallel or perpendicular to the flavin of FAD.

FAD and is compared with the position of the duroquinone in the original crystal structure. The docked duroquinone twists very slightly from the original position, but the two still match well. The RMS difference in the positions of the carbon and oxygen atoms in the docked and original duroquinones is 0.12 Å. Considering the ensemble property of the crystal structure and the uncertainties in the crystal coordinates ( $R$ -value = 0.202), the docking calculations

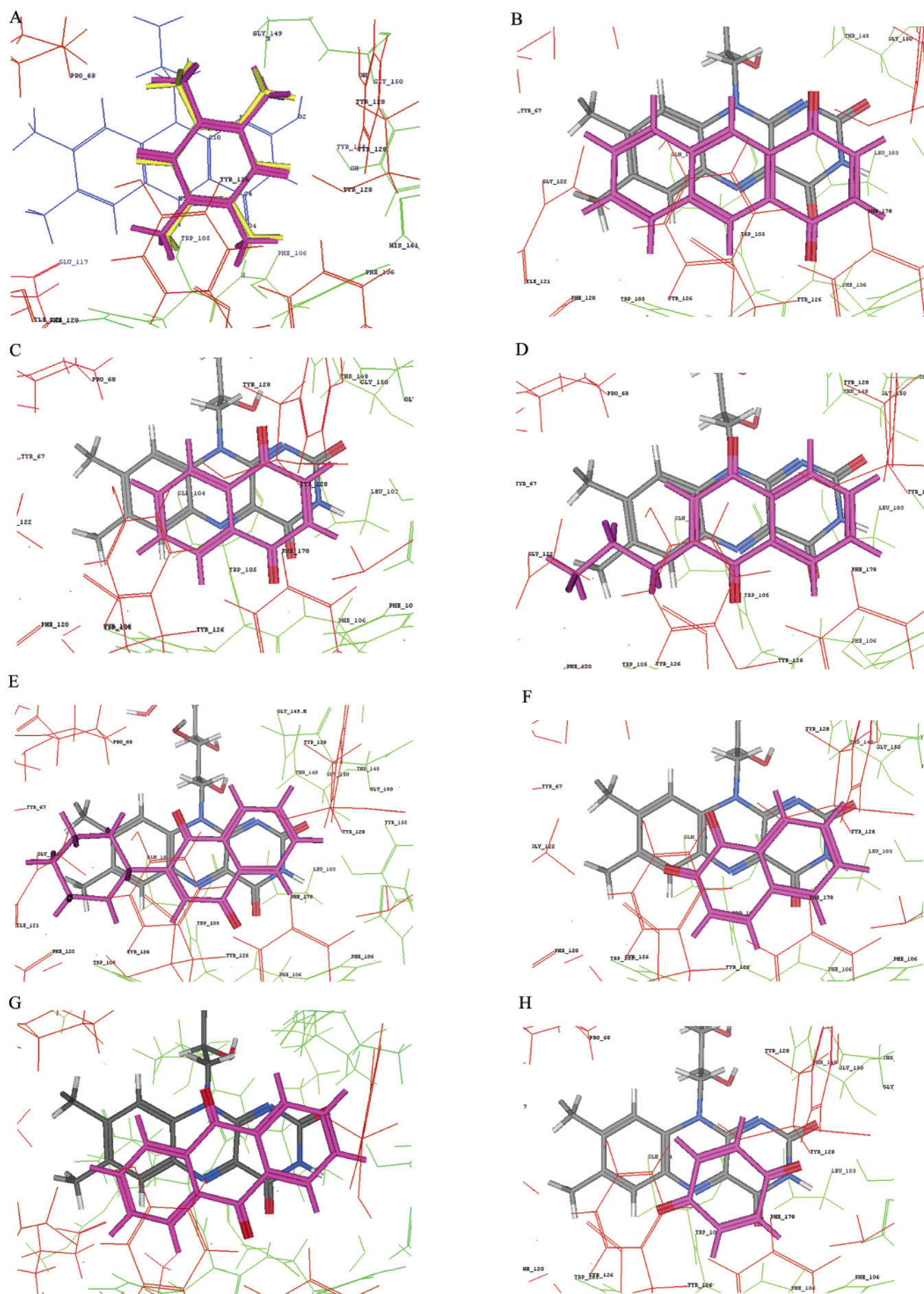
reproduced the crystal structure very well. In both the docked and original structures, there is a hydrogen bond between the carbonyl oxygen of duroquinone and the Tyr126 hydroxyl group.

**Docking Results for Other Quinones.** The lowest energy MOE-docked structures for a total of nine quinones are shown in Figure 2. Three of the nine quinones, duroquinone, 1,4-anthraquinone, and 9,10-anthraquinone, gave results in which all 20 docked positions fell within a single cluster. There is, therefore, just one preferred binding orientation for each of these three quinones. In the docked structure for 1,4-anthraquinone ( $K_Q = 0.91 \mu\text{M}$ ), shown in Figure 2B, the quinone nucleus runs parallel to the three-ring nucleus of the flavin ring but is slightly offset, a positioning that has been shown to be energetically optimal for  $\pi$ -ring-stacking interactions (31). In the docked structure for 9,10-anthraquinone ( $K_i = 80 \mu\text{M}$ ) in Figure 2G, the quinone ring nucleus can be seen to be twisted away from the parallel orientation, decreasing the possible  $\pi$ -ring-stacking interactions.

For each of the five naphthoquinones, 1,4-naphthoquinone, 2-propyl-1,4-naphthoquinone, 2-cyclohexyl-1,4-naphthoquinone, 1,2-naphthoquinone, and 2,3-dimethyl-1,4-naphthoquinone, the 20 docked structures fall into two clusters having very different binding orientations. The lowest energy and usually most prevalent docked structures, found in cluster 1 for each quinone, are shown in panels C–F and I of Figure 2. For the 1,4-naphthoquinones, these structures yield quinone orientations that are parallel to the flavin ring. The higher energy docked structures for 1,4-naphthoquinone and 2-propyl-1,4-naphthoquinone, found in cluster 2, correspond to quinone orientations that are perpendicular to the flavin ring. As with 1,4-anthraquinone, the favored offset, parallel orientations of all 1,4-naphthoquinones maximize  $\pi$ -ring-stacking interactions with the flavin ring. For 2,3-dimethyl-1,4-naphthoquinone, these structures yield two orientations which are both parallel to the flavin ring but are opposite in direction. The two orientations have nearly the same docking energy.

In the case of the 1,2-naphthoquinone, the lowest energy structure is found in cluster 1, and this structure shows a quinone orientation that is twisted away from the parallel offset orientation of the 1,4-naphthoquinone. In fact, the orientation of the 1,2-naphthoquinone is similar to that found for 9,10-anthraquinone. The kinetic studies (Table 2) indicate that these two latter quinones have a weaker binding affinity than do 1,4-anthraquinone and 1,4-naphthoquinone. The docking studies, therefore, can be used to make the argument that the extent of  $\pi$ -ring stacking is an important determinant of ligand binding affinity.

Autodock3 results of 12 quinones are listed in Table 5. For most of the quinones, Autodock3 produced binding orientations that were similar to those from MOE dock. One exception was 1,4-naphthoquinone, for which Autodock3 produced two clusters. The low-energy cluster was similar to that found in MOE dock. The second cluster, higher in energy, oriented the 1,4-naphthoquinone in the same position but rotated 180° from the first cluster. RMSD differences in docked positions between Autodock3 and MOE dock are listed for all quinones in Table 5. Another exception was 1,4-benzoquinone, for which Autodock3 also produced two clusters. The major cluster has a big discrepancy (RMSD =





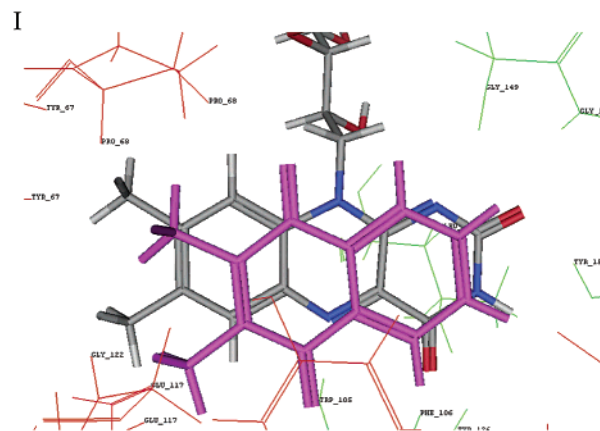


FIGURE 2: Orientations of MOE-docked quinones in the 1DXO active site relative to the FAD isoalloxazine ring: (A) duroquinone (the yellow color is the docked structure and the pink color is the crystal structure); (B) 1,4-anthraquinone; (C) 1,4-naphthoquinone; (D) 2-propyl-1,4-naphthoquinone; (E) 2-cyclohexyl-1,4-naphthoquinone; (F) 1,2-naphthoquinone; (G) 9,10-anthraquinone; (H) 1,4-benzoquinone; (I) 2,3-dimethyl-1,4-naphthoquinone.

6.41 Å) with the MOE-dock result (Figure 2H), while the minor cluster is very similar (RMSD = 1.06 Å) to the MOE-dock result. 1,4-Benzoquinone, as the smallest substrate in this study, has the greatest possible number of orientations within the active site. The MOE-docking results indicate that 1,4-benzoquinone is oriented above the N<sup>1</sup>–N<sup>3</sup> ring of the flavin in a position similar to that of duroquinone [the RMSD of common heavy atoms (six aromatic carbons + two oxygens) between docked benzoquinone and duroquinone is ~1.15]. Autodock in its major cluster, however, places 1,4-benzoquinone over the third ring (C<sup>6</sup>–C<sup>9</sup>) of the flavin. In this case, we think the MOE-dock results are more acceptable, as they are clearly more consistent with the kinetic data. The almost identical  $K_Q$  and maximal velocity values for 1,4-benzoquinone and duroquinone in Table 1 argue strongly for the almost identical positioning at the active site that is predicted by MOE dock.

**Binding Free Energy Calculations for MOE-Docked Quinones.** The relative binding free energies (BFE) of nine representative quinones, as calculated from their  $\Delta G_s$ ,  $\Delta G_a$ , and  $\Delta G_n$  components by methods described earlier, are listed in Table 6. It is clear that the nonelectrostatic component ( $\Delta G_n$ ) is the major contributor to the BFE. Although smaller, the widely varying assembly energies ( $\Delta G_a$ ) account for much of the BFE differences among the quinones. A correlation of BFE (Table 6) with  $\ln K_Q$  for the MOE-docked quinones was carried out as shown in Figure 3. The plot shows a good linear correlation ( $R^2 = 0.91$ ) between the calculated binding free energy and  $\ln K_Q$ . Autodock3 was also used to determine the relative binding free energies for all quinones, and the resulting correlation plot is shown in Figure 4.

By comparing Figures 3 and 4, we see that the quinone substrates fall into three distinct regions: weak binding ( $\ln K_Q = 4$ –5), intermediate binding ( $\ln K_Q = 1$ –2), and tight binding ( $\ln K_Q \approx 0$ ). While there is some variation within the regions, the trends in the calculated binding free energies generally support the trends seen in the kinetic  $K_Q$  values. We note that benzoquinone is consistently above the trend line and 2-cyclohexyl-1,4-naphthoquinone is below the trend line. In its native state, a protein has the flexibility to change its conformation to accommodate substrates of different sizes and shapes, but in the docking calculations we carried out,

the protein is held in the fixed position specified by the crystal structure. Thus, the smallest (benzoquinone) and largest substrates (2-cyclohexyl-1,4-naphthoquinone), requiring the greatest accommodation on the part of the enzyme, show deviations that are opposite in sign.

**Alkyl-Substituted 1,4-Naphthoquinones.** In its lowest energy docked state, unsubstituted 1,4-naphthoquinone binds to the QR1 active site with an orientation parallel to the flavin ring and with the carbonyl oxygen axis overlaying the N<sup>1</sup>–N<sup>3</sup> ring (ring to the right in our renderings) of the flavin (see Figure 2C). For the alkyl-substituted 1,4-naphthoquinones, however, two binding orientations of nearly equal energy are predicted by the docking studies. Orientation A shows the same ring positioning as 1,4-naphthoquinone (Figure 2C), but for most compounds in the series the ring is moved relative to the flavin such that the carbonyl axis tends to overlay the central N<sup>5</sup>–N<sup>10</sup> ring of the flavin. In orientation A, the alkyl groups project out to the right over the N<sup>1</sup>–N<sup>3</sup> ring. In orientation B (see Figure 2D,E,I), the quinone nucleus is flipped 180°, projecting the alkyl groups along the length of the flavin ring toward the far left ring of the flavin and placing the carbonyl oxygen axis predominantly over the N<sup>5</sup>–N<sup>10</sup> ring of the flavin.

Two characteristics are common to both predicted docked positions of all alkyl-substituted 1,4-naphthoquinones. First, almost all of the atoms in the quinone nuclei and their extended alkyl groups are localized directly over the isoalloxazine ring. Ring-to-ring  $\pi$ -stacking interactions are available in all binding orientations. Since the active site interactions, mainly  $\pi$ -ring stacking and van der Waals forces, are the same for the A and B orientations, we would expect both to predict similar binding affinities for the alkyl-substituted series. Second, orientations A and B both position the carbonyl axes of most of the alkyl-substituted quinones within a narrow ( $\pm 1.75$  Å) range over the central N<sup>5</sup>–N<sup>10</sup> ring of the flavin. It is therefore conceivable that the maximal velocities, which are expected to be dependent on the carbonyl positioning, could cluster within the narrow range seen in Table 3. Thus, although we are unable to conclusively prove either binding orientation, we consider both orientations A and B to be consistent with the kinetic data in Table 3.

Table 5: Energy and Position Difference between Several Best Docked Configurations of Each Substrate by Autodock3

	cluster	no. in cluster <sup>a</sup>	$\Delta E^b$ (kcal/mol)	RMSD <sup>c</sup> (Å)
benzoquinone 6.41 <sup>d</sup>	1	7	0.19 0.19 0.19 0.20	<0.10 0.20 0.20 0.26
1.06	2	3	0.10 0.14	0.12 0.21
duroquinone 1.78	1	7	0.09 0.09 0.10	<0.10 0.12 0.15
1,4-naphthoquinone 1.89	1	5	0.03 0.03 0.14	0.34 0.44 0.40
	2	5	0.19 0.26 0.35	0.78 0.34 0.53
1,2-naphthoquinone 1.04	1	5	0 0 0.01 0.01	<0.10 <0.10 <0.10 <0.10
2-cyclohexyl-1,4-naphthoquinone 0.81	1	6	0.05 0.37 0.38	0.30 0.11 <0.10
	2	4	0 0 0	<0.10 <0.10 <0.10
2-propyl-1,4-naphthoquinone 0.417	1	5	0.03 0.03 0.14 0.19	0.34 0.44 0.40 0.78
1,4-antraquinone 1.60	1	8	0 0.01 0.01 0.01	0.43 0.44 0.20 0.45
9,10-antraquinone 0.20	1	9	0.01 0.01 0.01 0.01 0.01	<0.10 <0.10 <0.10 <0.10 <0.10
2,3-dimethyl-1,4-naphthoquinone 0.84	1	13	0.01 0.01 0.01 0.01 0.04	<0.10 <0.10 <0.10 <0.10 <0.10
2-methyl-1,4-naphthoquinone	1	17	0 0.01 0.05 0.02	<0.10 <0.10 <0.10 <0.10
2-ethyl-1,4-naphthoquinone	1	16	0.08 0.04 0.05 0.02	0.21 <0.10 0.32 0.12
2-butyl-1,4-naphthoquinone	1	18	0.05 0.07 0.07 0.02	0.25 0.14 0.11 <0.10

<sup>a</sup> The number of configurations falling in the cluster. <sup>b</sup>  $\Delta E = E_i - E_{\text{lowest}}$ . <sup>c</sup> RMSD, root-mean-square deviation between the docked structure and the lowest energy docked structure. <sup>d</sup> The RMSD between quinones docked by Autodock3 and MOE dock. For benzoquinone, the major binding structure in Autodock is different from MOE-docking results, and the other is similar to MOE-docking results; see Docking Results for Other Quinones for detail. <sup>e</sup> Substrate is perpendicular to the flavin of FAD.

**Maximal Velocity Data and Docking Results.** Two factors related to substrate positioning at the active site are important in the analysis of maximal velocity patterns. The first is the distance between potential hydride donors ( $\text{N}^5$  and possibly  $\text{N}^1$ ) on the flavin ring and hydride acceptors on the quinone nucleus. Ultimately, both carbonyl oxygens of the quinone

Table 6: Calculated Relative Binding Free Energies, Solvation Energies, Assembly Energies, and Nonelectrostatic Solvation Energies (kcal/mol)

substrate	$\Delta G_s$	$\Delta G_a$	$\Delta G_n$	BFE <sup>a</sup>	$\ln K_Q$
1,4-benzoquinone	0.18	1.32	-4.66	-3.16	4.50
duroquinone	0.03	0.63	-4.96	-4.30	4.43
1,4-naphthoquinone	0.17	-0.91	-4.91	-5.65	1.10
1,2-naphthoquinone	0.17	1.01	-4.94	-3.76	4.41
2,3-dimethyl-1,4-naphthoquinone	0.18	-0.68	5.15	5.65	1.13
2-propyl-1,4-naphthoquinone	0.21	-0.89	-5.27	-5.95	1.28
2-cyclohexyl-1,4-naphthoquinone	0.19	-0.85	-5.40	-6.06	1.79
1,4-antraquinone	-0.37	-1.22	-5.17	-6.76	-0.094
9,10-antraquinone	0.25	-1.05	-5.21	-6.02	

<sup>a</sup> BFE, binding free energy by eq 1.

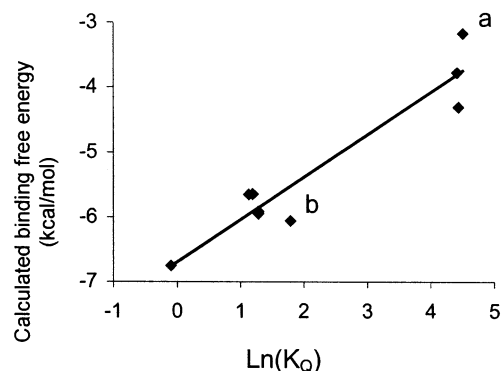


FIGURE 3: Calculated binding free energy (Poisson–Boltzmann method) by eq 1 of eight quinones in QR1 vs their experimental values ( $\ln K_Q$ ).  $R^2 = 0.9081$ . (a) Benzoquinone; (b) 2-cyclohexyl-1,4-naphthoquinone; others are duroquinone, 1,2-naphthoquinone, 1,4-naphthoquinone, 2,3-dimethyl-1,4-naphthoquinone, 2-*n*-propyl-1,4-naphthoquinone, and 1,4-antraquinone.

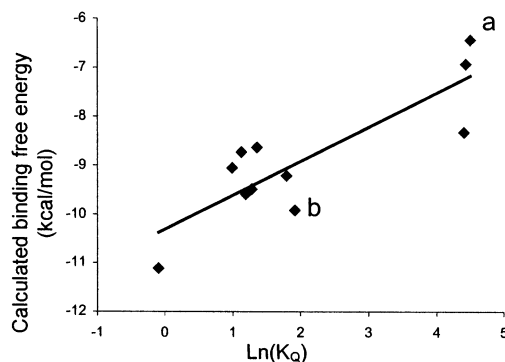


FIGURE 4: Calculated binding free energy (Autodock3) of 11 quinones in QR1 vs their experimental values ( $\ln K_Q$ ).  $R^2 = 0.7241$ . (a) Benzoquinone; (b) 2-cyclohexyl-1,4-naphthoquinone; others are duroquinone, 1,2-naphthoquinone, 1,4-naphthoquinone, 2-methyl-1,4-naphthoquinone, 2,3-dimethyl-1,4-naphthoquinone, 2-ethyl-1,4-naphthoquinone, 2-*n*-propyl-1,4-naphthoquinone, 2-*n*-butyl-1,4-naphthoquinone, and 1,4-antraquinone.

substrate and all carbons in the quinone ring are possible sites of hydride attack. A second factor is the positioning of Tyr126 and Tyr128 relative to the two carbonyl oxygens of the quinone. These tyrosines can serve as general acid catalysts, either alone or via a bridging water molecule, to protonate the negative intermediate produced by hydride attack. Because the two tyrosines reside on the highly flexible loop that serves as a lid for the active site, it is difficult via



modeling to predict their new positions when a different substrate is introduced into the active site. The large number of possible hydride donor–acceptor combinations and the uncertainty in the positioning of the tyrosine general acids make any quantitative correlation of maximal velocity values and modeled quinone positions ambiguous and complex. We therefore can draw no certain conclusions regarding the modeled substrate positions and measured maximal velocities.

## CONCLUSION

Quinone reductase possesses broad substrate specificity, catalyzing the reduction of simple benzo-, naphtho-, and anthraquinones, as well as complex molecules such as benzimidazolidiones (32), anthraquinone-based antitumor agents (29), and vitamin E related compounds (33). This broad specificity is advantageous to the enzyme in its role as a general detoxification agent and for its potential use in the in situ bioreductive activation of quinone-based pharmacological agents (3). The work presented here seeks to elucidate how the QR1 active site accommodates substrates of different size and structure by studying the effect of adding fused aromatic rings and flexible alkyl substituents to the quinone nucleus.

The steady-state kinetic data demonstrate that the QR1 active site can accommodate quinones with one, two, and three fused rings and that, as the number of fused rings increases from 1 to 3, binding affinity increases 100-fold with a concomitant 8-fold decrease in maximal velocity. The kinetic data suggest that the larger quinones rotate along the quinone carbonyl axis, relative to the duroquinone position in the crystal structure, to provide optimal  $\pi$ -ring-stacking interactions with the isoalloxazine ring of the flavin.

The docking studies strongly support this interpretation of the kinetic results. The docked structures indicate that 1,4-naphthoquinone and 1,4-anthraquinone rotate their carbonyl positions ca. 90° from the position in duroquinone, producing a parallel, offset alignment of the quinone and flavin rings, thereby allowing strong  $\pi$ -ring-stacking interactions. The validity of the docked orientations is confirmed by the docking of the excised duroquinone into its original position in the crystal structure and by the strong correlation between calculated binding energies for the docked orientations and experimentally determined  $K_Q$  values.

The kinetic effect of adding flexible alkyl groups to the quinone nucleus is much smaller than for adding additional fused rings. For the 1,4-naphthoquinone system, Michaelis constants and maximal velocities vary only within a factor of 2. The docking studies show that the alkyl groups lie, together with the naphthoquinone nucleus, along the entire length of the flavin ring in a parallel orientation. Apparently, enough room is available along the flavin axis to accommodate alkyl groups of up to the six carbons used in this study.

## ACKNOWLEDGMENT

The authors thank Dr. Alexander D. MacKerrell, Jr., of the University of Maryland School of Pharmacy for calculating free energies of aqueous solvation of the quinone substrates in Table 1.

## REFERENCES

1. Faig, M., Bianchet, M. A., Chen, S., Winski, S., Ross, D., Talalay, P., and Amzel, L. M. (2000) Structures of Recombinant Mouse and Human Nad(P)H:Quinone Oxidoreductases: Species Comparison and Structural Changes with Substrate Binding and Release, *Proc. Natl. Acad. Sci. U.S.A.* 97, 3177–3182.
2. Iyanagi, T., and Yamazaki, I. (1970) One electron transfer reactions in biochemical systems. V. Difference in the mechanism of quinone reductase by the NADH dehydrogenase and the NAD(P)H dehydrogenase (DT-diaphorase), *Biochim. Biophys. Acta* 216, 282–294.
3. Ross, D., Kepa, J. K., Winski, S. L., Beall, H. D., Anwar, A., and Siegel, D. (2000) NAD(P)H:quinone oxidoreductase 1 (NQO1): chemoprotection, bioactivation, gene regulation and genetic polymorphisms, *Chem.-Biol. Interact.* 129, 77–97.
4. Li, R., Bianchet, M. A., Talalay, P., and Amzel, L. M. (1995) The three-dimensional structure of NAD(P)H:quinone reductase, a flavoprotein involved in cancer chemoprotection and chemotherapy: mechanism of the two-electron reduction, *Proc. Natl. Acad. Sci. U.S.A.* 92, 8846–8850.
5. Skelly, J. V., Sanderson, M. R., Suter, D. A., Baumann, U., Read, M. A., Gregory, D. S. J., Bennett, M., Hobbs, S. M., and Neidle, S. (1999) Crystal structure of human DT-diaphorase: a model for interaction with the cytotoxic drug 5-(Aziridin-1-yl)-2,4-dinitrobenzamide (CB1954), *J. Med. Chem.* 42, 4325–4330.
6. Smith, L. I., and Webster, I. M. (1937) The reaction between quinones and sodium enolate. V. 2,3-dimethylnaphthoquinone and sodium malonic ester, *J. Am. Chem. Soc.* 59, 662–667.
7. Prochaska, H. J. (1988) Purification and crystallization of rat liver NAD(P)H:(quinone-acceptor) oxidoreductase by cibacron blue affinity chromatography: identification of a new and potent inhibitor, *Biochem. Biophys.* 267, 529–538.
8. Hosada, S., Nakamura, W., and Hayashi, K. (1974) Properties and Reaction mechanism of DT Diaphorase from Rat Liver, *J. Biol. Chem.* 249, 6416–6423.
9. Prochaska, H. J., and Santamaria, A. B. (1988) Direct measurement of NAD(P)H:quinone reductase from cells cultured in microtiter wells: a screening assay for anticarcinogenic enzyme inducers, *Anal. Biochem.* 169, 328–336.
10. Cossi, M., Barone, V., Cammi, R., and Tomasi, J. (1996) Ab initio study of solvated molecules: a new implementation of the polarizable continuum model, *Chem. Phys. Lett.* 255, 327–335.
11. Tomasi, J., and Perisco, M. (1994) Molecular interactions in solution: an overview of methods based on continuous distributions of the solvent, *Chem. Rev.* 94, 2027–2094.
12. Morris, G. M., Goodsell, D. S., Halliday, R. S., Huey, R., Hart, W. E., Belew, R. K., and Olson, A. J. (1998) Automated Docking Using a Lamarckian Genetic Algorithm and Empirical Binding Free Energy Function, *J. Comput. Chem.* 19, 1639–1662.
13. Morris, G. M., Goodsell, D. S., Huey, R., Hart, W. E., Halliday, R. S., Bellow, R., and Olson, A. J. (2000) Autodock3 User Guide, p 10, Scripps, La Jolla, CA.
14. Solis, F. J., and Wets, R. J. (1981) Minimization by Random search techniques, *Math. Oper. Res.* 6, 19–30.
15. Gilson, M. K., and Honig, B. (1991) The inclusion of electrostatic hydration energies in molecular mechanics calculations, *J. Comput.-Aided Mol. Des.* 5, 5–20.
16. Gilson, M. K., McCammon, J. A., and Madura, J. D. (1995) Molecular dynamics simulation with a continuum electrostatic model of the solvent, *J. Comput. Chem.* 16, 1081–1095.
17. Baginski, M., Polucci, P., Antonini, I., and Martelli, S. (2002) Binding free energy of selected anticancer compounds to DNA-theoretical calculations, *J. Mol. Model.* 8, 24–32.
18. Jorgensen, W. L., Duffy, E. M., Essex, J. W., Severance, D. L., Blake, J. F., Jones-Hertzog, D. K., Lamb, M. L., and Tirado-Rives, J. (1997) Approaches to protein–ligand binding from computer simulations, *NATO ASI Ser., Ser. E* 342, 21–34.
19. Massova, I., and Kollman, P. A. (2000) Combined molecular mechanical and continuum solvent approach (MM-PBSA/GBSA) to predict ligand binding, *Perspect. Drug Discovery Des.* 18, 113–135.
20. Nicholls, A., and Honig, B. (1991) A rapid finite difference algorithm, utilizing successive over-relaxation to solve the Poisson–Boltzmann equation, *J. Comput. Chem.* 12, 435–445.
21. Sitkoff, D., Sharp, K. A., and Honig, B. (1994) Accurate Calculation of Hydration Free Energies Using Macroscopic Solvent Models, *J. Phys. Chem.* 98, 1978–1988.

22. Zhou, Z., Madrid, M., and Madura, J. D. (2002) Docking of Non-nucleoside Inhibitors: Neotripterifordin and its Derivatives to HIV-1 Reverse Transcriptase, *Proteins: Struct., Funct., Genet.* 49, 529–542.
23. Esposito, E. X., Baran, K., Kelly, K., and Madura, J. D. (2000) Docking substrates to metalloenzymes, *Mol. Simul.* 24, 239–306.
24. Esposito, E. X., Baran, K., Kelly, K., and Madura, J. D. (2000) Docking of sulfonamides to carbonic anhydrase II and IV, *J. Mol. Graphics Modell.* 18, 283–289.
25. Weiner, S. J., Kollman, P. A., Case, D. A., Singh, U. C., Ghio, C., Alagona, G., Profeta, S., and Weiner, P. (1984) A New Force Field for Molecular Mechanical Simulation of Nucleic Acids and Proteins, *J. Am. Chem. Soc.* 106, 765.
26. Hall, J. M., Lind, C., Golvano, M. P., Rase, B., and Ernster, L. (1972) in *Structure and Function of Oxidation Reduction Enzymes* (Akeson, A., and Ehrenberg, A., Eds.) pp 433–443, Pergamon Press, Oxford.
27. Chen, H. H., Ma, J. X., Forrest, G. L., Deng, P. S., Martino, P. A., Lee, T. D., and Chen, S. (1992) Expression of rat liver NAD(P)H:quinone-acceptor oxidoreductase in *Escherichia coli* and mutagenesis in vitro at Arg-177, *Biochem. J.* 284, 855–860.
28. Zhou, Z., and Swenson, R. P. (1996) The cumulative electrostatic effect of aromatic ring stacking interactions and the negative electrostatic environment of the flavin mononucleotide binding site is a major determinant of the reduction potential for the flavodoxin from *Desulfovibrio vulgaris*, *Biochemistry* 35, 15980–15988.
29. Fisher, G. R., Gutierrez, P. L., Oldcorne, M. A., and Patterson, L. H. (1992) NAD(P)H (quinone acceptor) oxidoreductase (DT-diaphorase)-mediated two-electron reduction of anthraquinone-based antitumor agents and generation of hydroxyl radicals, *Biochem. Pharmacol.* 43, 575–585.
30. Chen, S., Knox, R., Wu, K., Deng, P. S.-K., Zhou, D., Bianchet, M. A., and Amzel, L. M. (1997) Molecular Basis of the catalytic differences among DT-diaphorase of Human, Rat and Mouse, *J. Biol. Chem.* 272, 1437–1439.
31. Hunter, C. A., and Sanders, K. M. (1990) The nature of  $\pi$ - $\pi$  interactions, *J. Am. Chem. Soc.* 112, 5525–5534.
32. Suleman, A., and Skibo, E. B. (2002) A Comprehensive Study of the Active Site Residues of DT-Diaphorase: Rational Design of Benzimidazolidiones as DT-Diaphorase Substrates, *J. Med. Chem.* 45, 1211–1220.
33. Siegel, D., Bolton, E. M., Burr, J. A., Liebler, D. C., and Ross, D. (1997) The reduction of alpha-tocopherolquinone by human NAD(P)H:quinone oxidoreductase: the role of alpha-tocopherol-hydroquinone as a cellular antioxidant, *Mol. Pharmacol.* 52, 300–305.

BI026518S